Available online at www.sciencedirect.com

SciVerse ScienceDirect

Procedia Engineering 19 (2011) 209 – 221

Procedia Engineering

www.elsevier.com/locate/procedia

1st CIRP Conference on Surface Integrity (CSI)

Recent Assessment of Surface Integrity Resulting from Fine Finishing Processes

M. J. Klopfstein[a]* and D. A. Lucca[b]

[a] *Manhattan College, 4513 Manhattan College Parkway, Riverdale, NY 10471, USA*
[b] *Oklahoma State University, 218 Engineering North, Stillwater, OK 74078, USA*

Abstract

This paper presents a variety of surface and subsurface characterization techniques for workpieces prepared by fine finishing processes which are beginning to emerge as useful tools. Further a summary of examples from the recent literature on the nature of the near surface produced by various processes is provided. Despite the availability of new characterization techniques most of the examples from the literature use older, well-developed techniques.

Selection and peer-review under responsibility of Prof. E. Brinksmeier

Keywords: Surface integrity, Measurement, Process

1. Introduction

There continues to be significant interest in assessing the near surface state produced by fine finishing processes. Whereas our ability to create finely finished surfaces by fine grinding, machining and polishing has improved, it is somewhat surprising that characterization of such surfaces still mainly relies on very well developed and long-used techniques (e.g., x-ray diffraction, taper sectioning, etc.). In this paper we briefly present a range of surface and subsurface characterization techniques which have seen limited use or are beginning to emerge as useful tools. After which, we survey the recent literature for reports on the nature of the near surface created by a variety of fine finishing processes. No attempt has been made to be complete or all inclusive, but rather to examine the surface state of metals, ceramics and single crystals which has been generated by current fine finishing processes.

* Corresponding author. Tel.: +001-718-862-7144; fax: +001-718-862-7163.
E-mail address: matthew.klopfstein@manhattan.edu.

doi:10.1016/j.proeng.2011.11.103

2. Techniques of Near Surface Evaluation

The literature contains extensive coverage of the various techniques which have been used for surface and near surface characterizations. Examples include a 1998 CIRP keynote paper [1] and a NASA Technical Report [2]. In Table 1 we have listed a few techniques which have seen limited use or are beginning to emerge as useful tools. A brief description of these techniques follows.

Optical techniques include methods which measure the transmission or reflection of incident light, the spectral content of the re-emitted light or the diffraction of x-rays. In the quasi-Brewster angle technique (qBAT) or variable angle spectroscopic ellipsometry [3 ,4, 5] surface and subsurface condition is quantified by observing the phase change of p-polarized light near the Brewster angle. Another technique to investigate the damage to optical components by high power lasers uses the percent of light transmittance to measure scattering from the damage [5].

Scanning confocal microscopy is emerging as a very useful tool for the characterization of the surface and subsurface of a variety of materials. Monochromatic light is directed to the surface and either the reflected light (reflection mode) [6 ,7] or the re-emitted light from excitation (fluorescence mode) [6, 8, 9, 10] is collected. The laser light is scanned over the surface providing a two-dimensional map of the collected light. Depth profile information is obtained by using the confocal capability of the microscope where the incident light is focused on or below the surface and only light from that focal point is collected using a confocal pin-hole. The material under investigation must be transparent to the incident light. Typical lateral spatial resolution and depth resolution is limited to about 1 μm. When used in reflection mode the intensity of the reflected light is measured, and the method can provide information about defects or scattering sites below the surface. The fluorescence mode (confocal fluorescence microscopy) collects the spectrally resolved re-emitted light and uses changes in peak amplitudes or spectral shifts to provide information on chemical species and residual stress.

X-ray diffractometry for the characterization of near surface microstructure and residual stresses of manufactured surfaces has long been employed. More recently, the use of high resolution x-ray diffractometry and x-ray topography for the study of single crystals has emerged. Whereas diffractometry examines the variation of total scattered intensity from a region which has been illuminated by an x-ray beam as a function of angle, topography (sometimes referred to as x-ray diffraction imaging) examines the spatial distribution of the scattered intensity as a function of position across the incident beam [11]. The technique is sensitive to individual crystal defects and lattice strain. The method is limited to a spatial resolution of about 1 μm. When used in a grazing incidence geometry, the technique can be employed to examine the near surface of crystals from tens of nanometers up to a micrometer. It has been successfully used to detect near surface damage produced by ultrafine finishing.

Focused ion beam (FIB) tomography has proven to be a powerful method for the 3-D imaging of microstructures in the 50 nm to 20 μm range [12]. Serial two dimensional cross-sectioning is performed in a system containing both a focused ion beam (for milling) and a scanning electron beam (for imaging). Often, a metallic film is deposited on the material under investigation to “establish” the surface [13]. Sputtering (or milling) is then performed with metallic ions (e.g., 30 kV Ga^{+}) perpendicular to the surface. The 2-D section is then imaged by an electron beam at a tilt angle of 45-55 degrees to the cross-section. Imaging can also be performed using the ion-induced secondary electrons [14]. The 2-D sections are then analyzed using specialized software to generate information on the 3-D volume. Another near surface characterization method which takes advantage of the milling capabilities of the FIB is energy filtering transmission electron microscopy (EFTEM) [15]. Using the method, chemical analysis of the near surface (e.g., microelectronics interconnects) can be performed with nanometer spatial resolution. The area of the surface of interest is first prepared by thinning using the FIB to thicknesses in the range of 100 nm. Compositional mapping is then performed using EFTEM which is based on imaging of core level

ionization edges. In this way, diffusion or compositional changes over nanometer spatial scales can be obtained.

Table 1. Description of techniques for the evaluation of the near surface

Technique	Principle	Nature of Surface Alteration Detected	Material Requirements	Reference
Optical/X-ray Techniques				
Quasi-Brewster	alterations in near surface causes changes in refractive index which shifts Brewster angle	Porosity	Transparent materials	3, 4
Scanning Laser Microscopy	scanning confocal microscopy at different depths to build a 3-D image; defects scatter more light than perfect material so appear bright in image	Cracks, contamination	Transparent materials	7
Confocal Fluorescence Microscopy	shift in Raman spectra of substitutional chromium ions in alumina with applied stress	Residual stress	Transparent materials	6, 8 - 10
Optical Transmittance	increased scattering from imperfections in crystal lattice reduce transmittance	Porosity, cracks	Transparent materials	5
X-ray Topography	diffraction of X-rays	Strain field	Single crystal materials	11
Transmission Electron Microscopy				
Energy Filtering TEM	use of magnetic prism and electromagnetic lenses to filter transmitted electrons; chemical analysis with nanometer spatial resolution obtained	Contamination	Workpiece must be able to be thinned to be transparent to electrons	15
Focused Ion Beam (FIB)				
FIB Tomography	imagining of surface using ion-induced secondary electrons; combined with FIB machining to obtain images normal to the surface	Surface topography	Conductive or moderately conductive surfaces or coated with conductive material	12 - 14
Acoustic Techniques				
Scanning electron acoustic microscopy (SEAM)	use of a chopped electron beam in an SEM to rapidly heat/cool sample which generates acoustic wave in material	Cracks, voids, delamination of film	Workpiece must be able to be thinned to about 2 mm thickness	16
Rutherford Backscattering in Channeling Configuration				
RBS-c	ion beam incident on aligned workpiece and energy of backscattered ions obtained	“Obstruction”-type and “distortion”-type defects	Single crystal materials	17

Scanning acoustic microscopy (SAM) is a well-known technique for investigating the near surface of materials for cracks, flaws, delaminations, etc. However as a result of typical Rayleigh wavelengths in crystalline materials of 10-20 μm, depth resolution is limited. A less employed variation of this technique is scanning electron acoustic microscopy (SEAM) [16]. The technique uses a pulsed electron beam to generate elastic waves in the near surface of the material under investigation. The electron beam of a typical scanning electron microscope is used. The depth resolution depends on the energy of the incident electron beam and the material under investigation, however can range from below 1 μm up to 5 μm. For

typical chopping frequencies of hundreds of kHz, the principal contrast is achieved by the generation of the acoustic wave as opposed to the propagation of the wave through the material as for the case of SAM. The technique has been shown to be particularly useful in identifying debonding and cracks in thin films.

Rutherford Backscattering Spectrometry (RBS) is a well-established technique for probing surface and near surface atomic composition. When employed such that the incident beam is aligned with one of the principal planes of symmetry of a single crystal (channeling conditions) RBS-c can provide information about both atomic composition and crystal structure. Applications have included the study of the lattice position of impurities of crystalline solids, the study of the nature of crystalline or amorphous thin films, and quantitative information about the subsurface damage of finely finished single crystals [17]. Channeling is achieved with ions having MeV energies. The high energy, light particles used (e.g., H or He ions) can penetrate deeply into the crystal without significant surface damage. As the beam encounters the crystal, some ions make close impact with the atoms at the surface, and experience large angle scattering events. The majority, however, are able to penetrate the crystal. If the crystal contains a thin, disordered or amorphous layer, the scattering yield at the surface increases over that for an undamaged, aligned crystal. If the layer is thin enough, some ions can make their way through the disordered layer, and will encounter ordered structure below. In this case, the backscattered yield will decrease, and a measure of the thickness of the disordered layer based on energy loss can be made. The technique can typically be used for investigating depths less than 1 μm from the surface. Grazing incidence scattering geometry allows for enhanced depth resolution such that depths as shallow as 20 nm can be investigated.

3. Examples of Near Surface Alterations in Materials

The nature and extent of near surface alterations caused by manufacturing processes can vary significantly depending on the type of process and the material. It is convenient to divide the class of all materials up into the broad categories of metals, ceramics and glasses and single crystal materials because of the distinct mechanical behavior of these materials. Table 2 provides examples of the nature and extent of near surface alterations for materials in each of the three classes. The next sections provide brief details of the references given in the table.

3.1 Metals

The most common techniques used to investigate the near surface of metals include metallographic preparation and etching, x-ray stress analysis and cross-sectional TEM. The types of near surface alterations typically considered are residual stress, dislocations, a heat affected layer or the formation of a "white" layer. Because of its continued prominence in manufacturing, the near surface of steels has been studied significantly. Ekmekci et al. [18] studied the electrical discharge machining (EDM) of blind holes in steel (1.2738). They produced holes using micro-EDM with a diameter of approximately 450 μm and depth of approximately 2000 μm. The surface of the hole was found to contain distinct layers which included a white layer, a carbon-enriched recast layer, an untempered martensitic layer and an overtempered martensitic layer. It was found that the total thickness of these layers was a function of the pulse energy with higher energy producing a thicker heat affected layer. The thickness of the layer ranged from approximately 1.5 – 4 μm. Ghanem et al. [19] measured the thickness of the white layer produced by EDM of two hardenable steels (X155CrMoV12 and C90) and two non-hardenable steels (X2CrNiMo17-12-02 and X6Cr17). The workpieces were machined with a graphite tool with a discharge voltage of 46 V and discharge intensity of 2 – 50 A. In the case of the hardenable steels it was found that a white layer extended from 5 μm to 80 μm beneath the surface. Under the white layer, a quenched layer

Table 2. The nature and extent of near surface alterations for various manufacturing processes and materials

		Surface Alteration		
Workpiece	Process	Nature	Extent	Reference
Metals				
Steel, 1.2738	Micro-EDM	Heat affected layer	1.5 – 4 µm	18
Steels (X155CrMoV12, C90, X2CrNiMo 17-12-2, X6Cr17)	EDM	White layer	5 – 80 µm	19
AISI 52100 steel	Hard turning	White layer	4.5 – 7.5 µm	20
AISI H11	Hard turning	Residual stress	200 µm	21
	Hard turning and shot peening	Residual stress	300 – 500 µm	21
	Hard turning and deep rolling	Residual stress	500 µm	21
	Hard turning and EDM	Residual stress	100 µm	21
Ni-based superalloy CG RR1000	Drilling and plunge milling	Axial residual stress	25 – 80 µm	22
Ni-Ti Alloy (SMA)	EDM	Melted layer	8 – 20 µm	23
Ti-384 and Ti-6Al-4V	High-speed milling	Dislocations	30 – 50 µm	24
Ti-2.5Cu	Shot peening	Residual stress	> 350 µm	25
	Ball-burnishing	Residual stress	> 350 µm	25
	Laser shock peening	Residual stress	> 350 µm	25
	Ultrasonic shot peening	Residual stress	300 µm	25
Ceramics and Glasses				
Alumina	High-speed grinding	Chipped layer	10 – 12 µm	26
Alumina	Grinding	Residual stress	28 – 37 µm*	27
Alumina-Titania	High-speed grinding	Chipped layer	10 – 12 µm	26
BK7	Grinding with ELID	Crack depth	3 µm	28
BK7	Grinding and lapping	Crack depth	up to 100 µm	29
BK7	Lapping	Crack depth/Craters	4 – 18 µm	30
BK7	Grinding	Crack depth	up to 2 µm	31
BK7	Grinding	Crack depth	up to 3.5 µm	32
Feldspar porcelain	Dental grinding	Cracks/porosity	up to 55 µm	33
Fused silica and fused quartz	Grinding with ELID	Crack depth	300 – 800 nm	34
Nd-doped phosphate glass	Grinding	Crack depth	4 – 32 µm	35
Nd-doped phosphate glass	Lapping and grinding	Crack depth	2 – 25 µm	36
SiC	Grinding	Chipped layer	5 – 7 µm	37
		Damage layer	9 – 12 µm	37
Silicon nitride	Grinding with ELID	Crack depth	0.4 – 1.3 µm	38
ULE and Zerodur	Grinding	Crack depth	6 – 16 µm	39
Yttria-Zirconia	High-speed grinding	Chipped layer	7 – 15 µm	26
Single Crystal Materials				
(111)$Cd_{0.96}Zn_{0.04}Te$	Chemomechanical polishing	Amorphous layer	~ 2 nm	40
HVPE GaN	Polishing	Dislocations	~60 nm	41
Germanium, p-type	Wire EDM	Crack depth	< 15 µm	42
(100)Si	Nanogrinding and chemo-mechanical-grinding	Amorphous layer	< 100 nm	43
		Dislocations	< 550 nm	43
(100)Si	Grinding	Amorphous layer and dislocations	40 – 70 nm	44
6H-SiC	Polishing	Dislocation loops	up to 400 nm	45
(100)ZnSe	Mechanical polishing	Dislocations	< 4 µm	46

* - depth calculated not measured

up to 80 μm thick and a transition layer up to a few μm thick were also found. In the case of the non-hardenable steels only a white layer was found. Schwach et al. [20] investigated the hard turning of steel and the white layer formed. The workpiece material was AISI 52100 steel which was heat treated to 61 – 62 HRC. The workpieces were face turned at a speed of 169.2 m/min, feed rate of 0.0254 mm/rev, and a depth of cut of 0.254 mm. They found a white layer that was 4.5 μm to 7.5 μm thick under which was a dark layer that was approximately 20 – 50 μm thick. The white layer exhibited a higher measured hardness than the bulk material and the dark layer had a lower measured hardness than the bulk material. The presence of the white layer was found to decrease the rolling contact fatigue life of the workpieces. Krauss and Scholtes [21] studied the near surface of AISI H11 steel because of the influence of the near surface on the thermal shock behavior of the steel. All workpieces were hard turned followed by either EDM, shot-peening, or deep rolling. Two types of shot-peening were investigated, coarse and fine, where the coarse used larger diameter balls and higher intensity. The hard turned workpiece had a compressive residual stress to a depth of about 200 μm. The deep rolled and coarse shot peened surfaces had compressive residual stresses to a depth of about 500 μm. The fine shot peened surface had a compressive residual stress to a depth of about 250 μm and the EDM workpiece had a tensile residual stress to about 100 μm. In thermal shock testing it was found that all the samples had a similar crack propagation rate. The authors attribute this to the combined effects of surface roughness, residual stress and microstructure of the material. To withstand the high temperatures of gas turbines, nickel-based superalloys are often employed. Kwong et al. [22] investigated the coarse grained alloy RR1000 to find the residual stress from making holes by drilling and plunge milling under various cutting conditions. Four cutting conditions were based on material removal rate and tool wear. The baseline cutting condition produced little tool wear but low material removal. Two other conditions were high speed and hence high material removal, and high wear conditions. The fourth cutting condition was without coolant and was meant as a worst-case scenario. The diameter of the hole was about 5 mm and the depth was 6 mm. The axial residual stress, that is along the axis of the hole, was found to be tensile for the baseline case and compressive for the other cases. For the baseline cutting condition, the residual stress extended about 25 μm beneath the surface whereas for the others it extended about 80 μm. Theisen and Schuermann [23] investigated the near surface of a nickel-titanium shape memory alloy after EDM. The experiments were performed on austenitic NiTi-SMA using EDM with frequencies of 5 or 10 kHz and working currents of 2 – 6 A. EDM produced a melted zone that ranged in thickness from 8 to 20 μm where higher values were obtained for the higher frequency and higher working currents. The melted zone contained a number of TiC precipitates. Thomas et al. [24] studied the high-speed milling of titanium Ti-834 which had approximately 80% by volume primary alpha grains. Figure 1 shows a backscattered electron micrograph of the cross-section of one of the workpieces. Slip bands which are visible at the top of the image were found to extend 30 to 50 μm below the surface and the intensity of the slip bands was higher on the crystals which were favorably aligned for slip. Maawad et al. [25] examined the effects of shot peening, ball burnishing, laser shock peening and ultrasonic shot peening on the residual stress of solution heat treated Ti-2.5Cu. They found that for all of the workpieces except the ultrasonic shot peened workpiece, residual compressive stress existed up to at least 350 μm which was the maximum depth investigated. The ultrasonic shot peened workpiece exhibited compressive residual stress to a depth of approximately 300 μm.

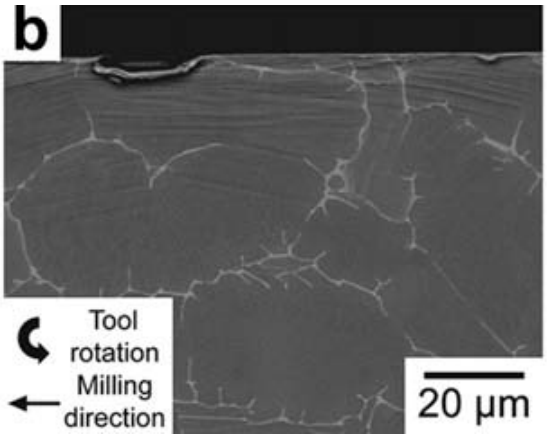

Fig. 1. Backscattered electron micrograph of cross sectioned titanium Ti-384 that was high-speed milled showing slip bands below the surface. From [24].

3.2 Ceramics and Glasses

Because of the brittle nature of these materials cracks and chipping of the material are often experienced during material removal processes. These two near surface alterations have received the most attention from researchers however near surface residual stress and porosity have also been investigated. The most common techniques to examine the near surface include: taper sectioning, cross-sectioning, optical microscopy and SEM. Huang and Liu [26] studied the effects of high speed grinding on the ceramics, alumina, alumina-titania and yttria partially stabilized tetragonal zirconia. Grinding was performed with a resin bonded diamond wheel with an average grit size of 160 µm with 100% concentration. Wheel speeds of 40 – 160 m/s were used in a down grinding mode. Chipping of the near surface was found to extend 7 – 15 µm beneath the surface and was only weakly related to the wheel depth of cut. Cavalieri et al. [27] studied the near surface of alumina and its response to grinding and subsequently its thermal shock behavior. Planetary grinding was performed using a resin bonded diamond wheel with 70 grit grains. They estimated the depth of compressive residual stress to be 28 – 37 µm. Zhao et al. [28] used electrolytic in-process dressing (ELID) grinding on BK7 glass and investigated the near surface for cracks. A specially developed coarse grained diamond wheel was used along with ELID. To measure the depth of cracks the workpiece was polished at a 45^{o} angle and the surface etched. Figure 2 shows an optical image of the surface where they found cracks up to a depth of 3 µm beneath the surface. Li et al. [29] also examined BK7 that had been ground or lapped. Grinding was performed with 250 µm or 125 µm grit at a cutting speed of about 20 m/s and a 20 µm depth of cut. Cracks in the material were found to penetrate to a depth of about 40 µm to 100 µm. Lapping experiments were performed with 20 µm diamond abrasive on a cast iron plate. Cracks were found to extend approximately 14 µm below the surface. Wang et al. [30] investigated the near surface of lapped BK7 workpieces. Silicon carbide abrasives were used where the size of the particles was 7 µm, 14 µm, 20 µm, 28 µm or 40 µm. Three different lapping plates were used, cast iron, aluminum and copper. The lapping pressure, velocity, and slurry concentration were also varied. The extent of cracks beneath the surface was found to depend strongly on the size of the abrasive used and the extent ranged from about 4 µm for the 7 µm abrasive particles to 18 µm for the 40 µm abrasive particles. Lapping plate hardness, lapping pressure, velocity and slurry concentration were found to only have a weak influence on the extent of crack depth. Zhao et al. [31] combined a hybrid copper-resin bonded grinding wheel with ELID in the grinding of BK7. The depth of cut was varied between 0.5 and 2 µm. Cracks were found to extend to a depth of 1 – 2 µm

beneath the surface. In horizontal surface grinding experiments on BK7, Gu et al. [32] used a resin bonded wheel with diamond abrasive with an average grain size of 5 μm.

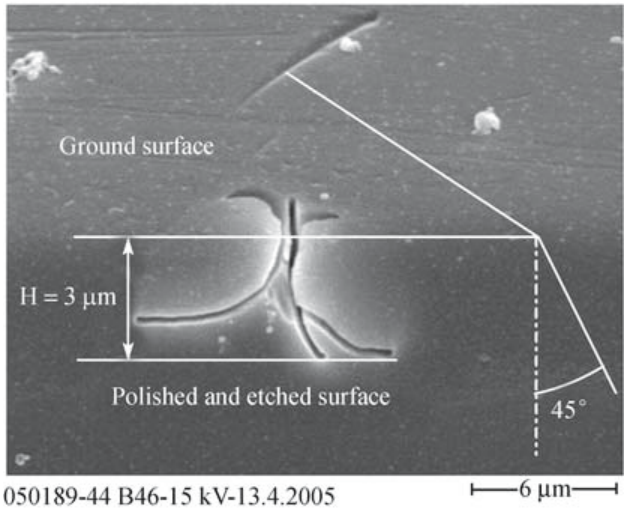

Fig. 2. Taper polished and etched surface of BK7 glass which had been ground using a coarse grained diamond wheel and ELID. From [28].

The depth of cut used was either 1 or 2 μm, the wheel speed was 20 m/s and the feed rate was varied between 2 and 80 mm/s. At the lowest feed rate, they were unable to detect any cracks beneath the surface and at the highest feed rate cracks were found up to about 3.5 μm below the surface. Song and Yin [33] studied the effects of grinding with dental tools on the near surface of feldspar porcelain. To ensure a good fit for dental ceramic prostheses the dentist typically performs minor grinding of the prosthesis using a diamond bur. This has been found however to cause premature failure of prostheses. Three different burs were used with grit sizes of: 106 – 125 μm, 53 – 63 μm and 20 – 30 μm. Cracks and an increase in the porosity of the material were observed to depths of 30 – 60 μm for the coarse grit bur, 20 – 35 μm for the medium grit bur and 3 – 8 μm for the fine grit bur. Zhao et al. [34] used a Tetraform 'C' machine to grind fused silica and fused quartz. ELID was used to dress the cup diamond grinding wheel with grain size of 6 – 12 μm. The peripheral speed of the wheel was held constant at 40 m/s, the feed speed was 6 mm/min and the depth of cut was 3 μm. They found that cracks propagated to a depth of 0.3 – 0.8 μm in the fused silica and up to a depth of 0.6 μm in the fused quartz. Zhang and Zhu [35, 36] investigated neodymium-doped phosphate glass which is often used in high peak power lasers. Cracks in the near surface of the glass can reduce the laser-induced damage threshold. Grinding was performed with diamond abrasives with average grit size from 7 – 20 μm. The depth of cracks beneath the surface was found to be between about 3 μm and 8 μm. Agarwal and Rao [37] performed surface grinding experiments on SiC using a resin bonded diamond grinding wheel with an average grit size of 121 μm. The wheel speed was 37 m/s, the feed rate was 5 m/min and the depth of cut was from 5 – 45 μm. The near surface exhibited a chipped layer and cracks. The chipped layer was caused mainly by grain dislodgement and was found to extend from 5 – 7 μm beneath the surface. Cracks were found to extend below this layer to a combined depth of 9 – 12 μm below the surface. Bandyopadhyay and Ohmori [38] investigated the use of ELID surface grinding on silicon nitride and the effects on the near surface. They used a grinding wheel velocity of 1200 m/min, feed of 20 m/min and a depth of cut of 5

μm. The grain size of the diamond wheel was from 5 – 10 μm to 0.5 – 3 μm. The depth of cracks was found to range from 0.4 μm to 1.3 μm where the shallowest depth was produced by the diamond wheel with the lowest grain size. Tonnellier et al. [39] investigate grinding of Zerodur and ULE glasses. Three different resin bonded diamond cup wheels with average grain size of 76 μm, 46 μm and 25 μm were used in the experiments. A grinding speed of 30 m/s was used for all experiments. The crack depth was measured by taper sectioning and etching. The crack depth in Zerodur was found to extend from 9.5 μm for the fine grinding wheel to 16 μm for the coarse grinding wheel. The crack depth in the ULE glass ranged from 6.6 μm for the fine grinding wheel to 17 μm for the coarse grinding wheel.

3.3 Single Crystal Materials

Single crystal materials are often used in opto-electronic devices which places stringent demands on the near surface. Dislocations or an amorphous layer in the near surface of these materials caused by processing can significantly limit the performance of a device made from such materials. Because of its widespread availability and the detailed information it provides, cross-sectional transmission electron microscopy is often used to examine the near surface of single crystal materials.

Zhang et al. [40] investigated the near surface of CdZnTe single crystals after chemomechanical polishing. The workpiece was (111)$Cd_{0.96}Zn_{0.04}Te$ and it was polished with a slurry containing silicon dioxide nanospheres with an average diameter of 5 nm and nitric, hydrochloric and lactic acids. The solution had a pH in the range of 2.6 – 3.2 and the duration of polishing was 12 minutes. The near surface was cross-sectioned and examined by high resolution TEM. It was found that there was an amorphous layer of about 2 nm in thickness on the surface and no other imperfections in the crystalline lattice were observed. Grandusky et al. [41] studied the effects of polishing on the near surface of GaN substrates and the subsequent changes in the performance of light emitting diodes (LED) grown on top of these workpieces. They obtained two sets of workpieces from vendors who used proprietary polishing processes. Although both workpieces were found to have low roughness values, they differed significantly in their photoluminescence and cathodoluminescence response. One of the workpieces had a more intense broad peak centered at about 377 nm which has been attributed to damage. Also the same sample exhibited reduced cathodoluminescence in a pattern that resembles polishing scratch marks. The authors suggest that dislocations during polishing act as point defect gettering sites. When LEDs were made from this workpiece it was found to have significantly lower intensity of light emission. Bamberg and Rakwal [42] investigated using wire electrical discharge machining (WEDM) to saw germanium. The germanium used was p-type that had been doped with gallium and the size of the workpieces was 15 mm x 2 mm x 2 mm. Brass and molybdenum wires were used with sizes ranging from 50 – 200 μm. The cross-section of the workpieces was examined by scanning electron microscopy. It was found that at low discharge energies no cracks were observed but at higher energies cracks were found to extend to about 15 μm below the surface. Huang et al. [43] used grinding and chemomechanical grinding on (100)Si. Face grinding was performed with diamond abrasive wheels with average grain size from 40 μm to 2 μm. Most experiments were performed with resin bonded wheels however the 2 μm grain size wheel was a vitreous bond. Chemomechanical grinding was carried out with cerium oxide abrasives in a resin bonded wheel where the average size of the grains was 2 μm. The near surface of the workpieces was examined using cross-sectional TEM. Grinding was found to produce an amorphous layer and dislocations in the near surface. The extent of the amorphous layer was about 100 nm for all grain sizes except for the 2 μm grain size wheel which produced an amorphous layer of a few nanometers. Dislocations were found beneath the amorphous layer and extended from 50 nm for the 2 μm abrasive to 400 nm for the 40 μm abrasive. The workpiece prepared by chemomechanical grinding was not found to have any imperfections in the near surface. Zhang et al. [44] performed face grinding experiments on

(100)Si using a diamond wheel with a specially made bond. The bonding material consisted of silicon carbide, alumina, silica and sodium chloride and the wheel was trued with a silicon carbide plate. The average grain size of the diamond abrasives was 0.9 μm. The wheel speed varied from 29 – 40 m/s, the workpiece speed was a constant 120 rpm and the feed rate varied from 1 to 10 μm/min. Cross-sectional TEM was used to examine the near surface. The top most layer was an amorphous layer under which was a damaged layer which contained dislocations. The total extent of these layers ranged from 40 – 70 nm beneath the surface. Grim et al. [45] investigated the mechanical polishing of 6H-SiC by plan view TEM. The workpieces were (0001) wafers which were intentionally off-cut at an angle of 8^{o} which is a standard off-cut. The surfaces were mechanically polished with 0.5 μm diamond abrasive slurry and for TEM preparation were thinned from the backside. TEM images show a series of dislocation half-loops which emanate from the scratches produced by polishing. The depth of the dislocations is estimated to be approximately 50 nm and the dislocation density is estimated to be on the order of 10^{10} cm^{-2}. Lucca et al. [46] studied the near surface of (100)ZnSe which had been mechanically polished. Surfaces were prepared with 0.25 μm or 1 μm diamond abrasive slurry. The near surface of the workpieces was evaluated by Rutherford backscattering in the channeling configuration (RBS-c) and by cross-sectional TEM. The RBS-c data indicated two types of damage present in the near surface: "obstruction"-type and "distortion"-type. Obstruction-type damage causes the direct backscattering of ions whereas distortion type damage causes a deflection of ions. For the workpieces prepared by either 0.25 μm or 1 μm diamond abrasive the extent of the obstruction type damage was found to be about 250 nm however the amount of damage was higher for the workpiece prepared with the 1 μm diamond abrasive. Distortion type damage was found to extend about 5 μm beneath the surface for both workpieces. Cross-sectional TEM confirmed these results, Figure 3. Figure 3(a) shows the near surface of a workpiece prepared using 0.25 μm diamond abrasive where there is a high density of damage that extends to a depth of 200 – 300 nm and Figure 3(b) shows that a few dislocations extend to a depth of about 4 μm beneath the surface.

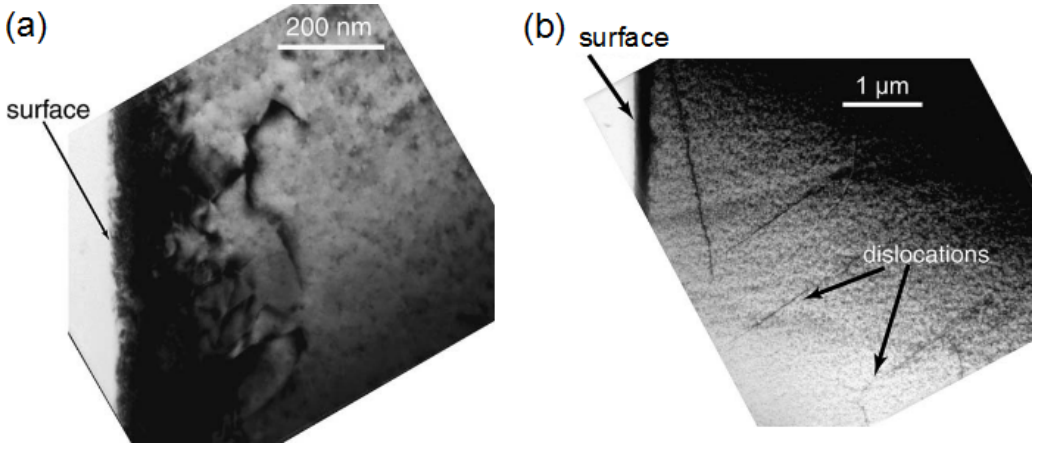

Fig. 3. Cross-sectional TEM images of (100)ZnSe prepared by mechanical polishing with 0.25 μm diamond abrasive. (a) shows a high density of damage in the near surface that extends 200 – 300 nm below the surface and (b) shows dislocations extending about 4 μm below the surface. From [46].

4. Summary

There exists a variety of techniques for assessing the near surface integrity of workpieces produced by fine finishing processes. This paper presented some of the emerging techniques and techniques that up to this point have seen limited use. Further, the paper presented examples from the recent literature of the nature and extent of near surface alterations produced by various processes. Despite the existence of newer, emerging techniques for the evaluation of the near surface, most all of these examples used well-developed techniques such as TEM, taper sectioning and x-ray diffraction. With the passage of time perhaps the emerging techniques of today will become the well-developed techniques of tomorrow.

References

[1] Lucca DA, Brinksmeier E, Goch G. Progress in assessing surface and subsurface integrity. *Annals of the CIRP* 1998; **47**:669-693.

[2] Miyoshi K. Surface characterization techniques: An overview. NASA Technical Report TM-2002-211497, 2002.

[3] Wang J, Maier RL. Surface assessment of CaF_2 deep-ultraviolet and vacuum-ultraviolet optical components by the quasi-Brewster angle technique. *Appl Optics* 2006;**45**:5621-8.

[4] Ma B, Shen Z, He P, Ji Y, Sang T, Jiao H et al. Subsurface quality of polished SiO2 surface evaluated by quasi-Brewster angle technique. *Optik* 2011;**122**:1418-1422.

[5] Wang J, Vankerkhove S, Schreiber H. Evaluation of coated and uncoated CaF_2 optics by variable angle spectroscopic ellipsometry. *Thin Solid Films* 2011;**519**:2881-4.

[6] Neauport J, Cormont P, Legros P, Ambard C, Destribats J. Imaging subsurface damage of grinded fused silica optics by confocal fluorescence microscopy. *Opt Express* 2009;**17**:3543-54.

[7] Fine KR, Garbe R, Gip T, Nguyen Q. Subsurface damage is measured nondestructively. *Laser Focus World* 2006;**42**:131-4.

[8] Guo S, Todd RI. Cr^{3+} microspectroscopy measurements and modelling of local variations in surface grinding stresses in polycrystalline alumina. *J Eur Ceramic Soc* 2010;**30**:2533-45.

[9] Guo S, Todd RI. Quantitative optical fluorescence microprobe measurements of stresses around indentations in Al_2O_3 and Al_2O_3/SiC nanocomposites: The influence of depth resolution and specimen translucency. *Acta Mater* 2011;**59**:2637-47.

[10] Wu HZ, Roberts SG, Derby B. Residual stress distributions around indentations and scratches in polycrystalline Al_2O_3 and Al_2O_3/SiC nanocomposites measured using fluorescence probes. *Acta Mater* 2008;**56**:140-9.

[11] Black D. Using X-ray topography to inspect surfaces of single-crystal components. *Int J Appl Ceram Tec* 2005;**2**:336-43.

[12] Elfallagh F, Inkson BJ. Evolution of residual stress and crack morphologies during 3D FIB tomographic analysis of alumina. *J Microsc* 2008;**230**:240-51.

[13] Wo PC, Munroe PR, Xie Z, Zhou Z, Li KY. Three-dimensional visualization of scratch-induced subsurface damage in TiSiN/TiN multilayer coating using focused ion beam–scanning electron microscopic tomography technique. *J Am Ceram Soc* 2011;**94**:1598-604.

[14] Wu HZ, Roberts SG, Möbus G, Inkson BJ. Subsurface damage analysis by TEM and 3D FIB crack mapping in alumina and alumina/5vol.%SiC nanocomposites. *Acta Mater* 2003;**51**:149-63.

[15] Pantel R, Torres J, Paniez P, Auvert G. Physical and chemical analysis of advanced interconnections using energy filtering transmission electron microscopy. *Microelectron Eng* 2000;**50**:277-84.

[16] Page TF, Shaw BA. Scanning electron acoustic microscopy (SEAM): A technique for the detection of contact-induced surface and sub-surface cracks. *J Mater Sci* 2004;**39**:6791-805.

[17] Lucca DA, Wetteland CJ, Misra A, Klopfstein MJ, Nastasi M, Maggiore CJ, Tesmer JR. Assessment of subsurface damage in polished II–VI semiconductors by ion channeling. *Nucl Instrum Meth B* 2004;**219-220**:611-7.

[18] Ekmekci B, Sayar A, Öpöz TT, Erden A. Geometry and surface damage in micro electrical discharge machining of micro-holes. *J Micromech Microeng* 2009;**19**:105030.

[19] Ghanem F, Braham C, Sidhom H. Influence of steel type on electrical discharge machined surface integrity. *J Mater Process Tech* 2003;**142**:163-73.

[20] Schwach DW, Guo YB. A fundamental study on the impact of surface integrity by hard turning on rolling contact fatigue. *Int J Fatigue* 2006;**28**:1838-44.

[21] Krauss M, Scholtes B. Thermal shock damage of hot-work tool steel AISI H11 in hard turned, electroeroded, shot-peened or deep rolled surface conditions. *J Mater Sci Technol* 2004;**20**:93-6.

[22] Kwong J, Axinte DA, Withers PJ. The sensitivity of Ni-based superalloy to hole making operations: Influence of process parameters on subsurface damage and residual stress. *J Mater Process Tech* 2009;**209**:3968-77.

[23] Theisen W, Schuermann A. Electro discharge machining of nickel–titanium shape memory alloys. *Mat Sci Eng A-Struct* 2004;**378**:200-4.

[24] Thomas M, Turner S, Jackson M. Microstructural damage during high-speed milling of titanium alloys. *Scripta Mater* 2010;**62**:250-3.

[25] Maawad E, Brokmeier HG, Wagner L, Sano Y, Genzel C. Investigation on the surface and near-surface characteristics of Ti–2.5Cu after various mechanical surface treatments. *Surf Coat Tech* 2011;**205**:3644-50.

[26] Huang H, Liu YC. Experimental investigations of machining characteristics and removal mechanisms of advanced ceramics in high speed deep grinding. *Int J Mach Tool Man* 2003;**43**:811-23.

[27] Cavalieri A, Míngolo N, Tomba Martinez A. Machining damage analysis of alumina in relation to thermal shock behavior. *J Mater Sci* 2010;**45**:3901-11.

[28] Zhao Q, Brinksmeier E, Riemer O, Rickens K. Ultra-precision ductile grinding of BK7 using super abrasive diamond wheel. *Front Mech Eng China* 2007;**2**:350-5.

[29] Li S, Wang Z, Wu Y. Relationship between subsurface damage and surface roughness of optical materials in grinding and lapping processes. *J Mater Process Tech* 2008;**205**:34-41.

[30] Wang Z, Wu Y, Dai Y, Li S. Subsurface damage distribution in the lapping process. *Appl Optics* 2008;**47**:1417-26.

[31] Zhao Q, Chen J, Yao J, Zhou S. Investigation of surface and subsurface damage in diamond grinding of optical glass using hybrid copper-resin-bonded diamond wheel. *J Vac Sci Technol B* 2009;**27**:1489-95.

[32] Gu W, Yao Z, Li H. Investigation of grinding modes in horizontal surface grinding of optical glass BK7. *J Mater Process Tech* 2011;**211**:1629-36.

[33] Song X-F, Yin L. The quantitative effect of diamond grit size on the subsurface damage induced in dental adjustment of porcelain surfaces. *P I Mech Eng H* 2010;**224**:1185-94.

[34] Zhao Q, Liang Y, Stephenson D, Corbett J. Surface and subsurface integrity in diamond grinding of optical glasses on Tetraform 'C'. *Int J Mach Tool Man* 2007;**47**:2091-7.

[35] Zhang W, Zhu J. Subsurface damage of Nd-doped phosphate glasses in optical fabrication. *Optik* 2008;**119**:738-41.

[36] Zhang W, Zhu J. Controlling subsurface damage in neodymium-doped phosphate glass. *Optik* 2009;**120**:752-7.

[37] Agarwal S, Rao PV. Experimental investigation of surface/subsurface damage formation and material removal mechanisms in SiC grinding. *Int J Mach Tool Man* 2008;**48**:698-710.

[38] Bandyopadhyay BP, Ohmori H. The effect of ELID grinding on the flexural strength of silicon nitride. *Int J Mach Tool Man* 1999;**39**:839-53.

[39] Tonnellier X, Morantz P, Shore P, Baldwin A, Evans R, Walker DD. Subsurface damage in precision ground ULE® and Zerodur® surfaces. *Opt Express* 2007;**15**:12197-205.

[40] Zhang Z, Meng Y, Guo D, Kang R, Gao H. Nanoscale machinability and subsurface damage machined by CMP of soft-brittle CdZnTe crystals. *Int J Adv Manuf Tech* 2010;**47**:1105-12.

[41] Grandusky JR, Jindal V, Tripathi N, Shahedipour-Sandvik F, Lu H, Kaminsky EB, Melkote R. Identification of subsurface damage in freestanding HVPE GaN substrates and its influence on epitaxial growth of GaN epilayers. *J Cryst Growth* 2007;**307**:309-14.

[42] Bamberg E, Rakwal D. Experimental investigation of wire electrical discharge machining of gallium-doped germanium. *J Mater Process Tech* 2008;**197**:419-27.

[43] Huang H, Wang BL, Wang Y, Zou J, Zhou L. Characteristics of silicon substrates fabricated using nanogrinding and chemo-mechanical-grinding. *Mat Sci Eng A-Struct* 2008;**479**:373-9.

[44] Zhang Z, Huo F, Wu Y, Huang H. Grinding of silicon wafers using an ultrafine diamond wheel of a hybrid bond material. *Int J Mach Tool Man* 2011;**51**:18-24.

[45] Grim JR, Benamara M, Skowronski M, Everson WJ, Heydemann VD. Transmission electron microscopy analysis of mechanical polishing-related damage in silicon carbide wafers. *Semicond Sci Tech* 2006;**21**:1709.

[46] Lucca DA, Shao L, Wetteland CJ, Misra A, Klopfstein MJ, Nastasi M. Subsurface damage in (100)ZnSe introduced by mechanical polishing. *Nucl Instrum Meth B* 2006;**249**:907-10.